VIP Biosensors Very Important Paper

International Edition: DOI: 10.1002/anie.201507354
German Edition: DOI: 10.1002/ange.201507354

Photocatalytically Renewable Micro-electrochemical Sensor for Real-Time Monitoring of Cells

*Jia-Quan Xu, Yan-Ling Liu, Qian Wang, Huan-Huan Duo, Xin-Wei Zhang, Yu-Tao Li, and Wei-Hua Huang**

Abstract: *Electrode fouling and passivation is a substantial and inevitable limitation in electrochemical biosensing, and it is a great challenge to efficiently remove the contaminant without changing the surface structure and electrochemical performance. Herein, we propose a versatile and efficient strategy based on photocatalytic cleaning to construct renewable electrochemical sensors for cell analysis. This kind of sensor was fabricated by controllable assembly of reduced graphene oxide (RGO) and TiO_2 to form a sandwiching RGO@TiO_2 structure, followed by deposition of Au nanoparticles (NPs) onto the RGO shell. The Au NPs-RGO composite shell provides high electrochemical performance. Meanwhile, the encapsulated TiO_2 ensures an excellent photocatalytic cleaning property. Application of this renewable microsensor for detection of nitric oxide (NO) release from cells demonstrates the great potential of this strategy in electrode regeneration and biosensing.*

Electrochemical sensors are wildly used in biosensing, because of their unique characteristics, such as fast response, excellent sensitivity, and high spatiotemporal resolution.[1] However, electrodes are easily fouled by intermediates or polymerization products generated by electrochemical reactions during the detection.[2] In particular, for real-time monitoring of cells on a planner electrode, on which cells were cultured,[3] secretions from the cells can lead to a severely contaminated electrode. The consequence of fouling and passivation is signal attenuation, resulting in unreliability and utilization decrease.[4]

Up to now, great effort has been made to improve the stability or refresh the surface of electrochemical sensors. For instance, anti-polymerization or anti-adsorption molecules could be chemically modified on electrode surfaces,[5] and fouling-resistant materials such as poly(3,4-ethylenedioxythiophene) and polypyrrole,[6] boron-doped diamond,[7] and carbon nanotubes[4b,8] have been used to construct electrochemical sensors. These methods can retard fouling and passivation to some extent, but the contaminant cannot be removed from the surface. Hence, to clear the pollutant away from the electrode surface, several other approaches were developed, including acid washing,[9] chemical oxidation or reduction,[9] and electrochemical oxidative or reductive cleaning,[10] but these methods would inevitably damage the sensors surface. Thus, it is still a great challenge to completely and efficiently remove the contaminant from the electrode surface without changing the surface structure and electrochemical performance.

As we know, photocatalysts such as TiO_2 and ZnO are a kind of material that can decompose the organic molecules by active oxygen radicals generated under ultraviolet irradiation without altering the surface morphology and structure,[11] which is widely used as photocatalytic cleaning material.[12] During the biochemical analysis, the main contaminants on the sensor surface were usually organic biomolecules. Hence, photocatalyst could be possibly used to construct refreshable electrochemical sensor which are cleaned by light. However, because of the low conductivity and poor electrochemical activity, photocatalysts are inappropriate for direct use as an electrochemical sensing material. To this end, photocatalysts are usually composited with noble metals or carbon materials to improve the sensing performance as well as to enhance the photocatalytic efficiency.[12b,13]

Herein, inspired by the excellent photocatalysis of TiO_2, high electric conductivity of graphene, and outstanding electrochemical performance of Au nanoparticles (NPs), we developed a kind of highly sensitive and photocatalytically renewable electrochemical sensor (Scheme 1 a–d). The renewable sensor was fabricated by controllable assembly of RGO and TiO_2 layer by layer via electrophoretic deposition on indium–tin oxide (ITO) to form a RGO@TiO_2 sandwich structure in situ, followed by decorating the RGO shell with Au NPs. Despite the sacrifice of some electrical conductance, graphene oxide (GO)/RGO is used here because of its superior electrochemical property, dispersibility, and functionalization relative to graphene.[13d] The Au NPs-RGO composite shell endows this sensor with high sensitivity, and a detection limit of 4 nM was obtained for detection of NO. Encapsulated TiO_2-based composites showed excellent properties when used for photocatalytic cleaning of absorbed polymers, proteins, and cell culture medium (CCM). These properties make it possible to recover culture and real-time monitoring of single cells on an engineered microsensor array (Scheme 1 d–f).

The preparation of the renewable electrode Au/RGO@TiO_2-ITO is illustrated in Scheme 1. Before the fabrication, anatase TiO_2 NPs with about 300 nm (Figure 1 a) diameter were prepared by sol–gel and hydrothermal method

[*] J.-Q. Xu, Y.-L. Liu, Q. Wang, H.-H. Duo, X.-W. Zhang, Dr. Y.-T. Li, Prof. W.-H. Huang
Key Laboratory of Analytical Chemistry for Biology and Medicine (Ministry of Education)
College of Chemistry and Molecular Sciences
Wuhan University, Wuhan 430072 (China)
E-mail: whhuang@whu.edu.cn

Supporting information for this article is available on the WWW under http://dx.doi.org/10.1002/anie.201507354.

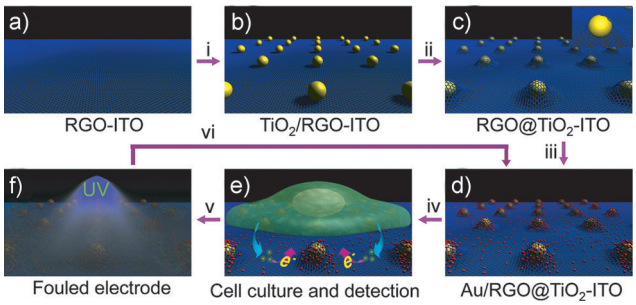

Scheme 1. Fabrication process of the renewable Au/RGO@TiO_2-ITO sensor and cell detection on the sensor. i) Deposition of TiO_2 NPs onto RGO-modified ITO (RGO-ITO) by electrophoresis. ii) TiO_2 NPs wrapped by RGO by electrostatic self-assembly. iii) Deposition of Au NPs by chemical reduction. iv) Cell culture and detection on the sensor. v) Fouled sensor after the cell was detached. vi) Sensor recovered by photocatalytic cleaning under UV light irradiation.

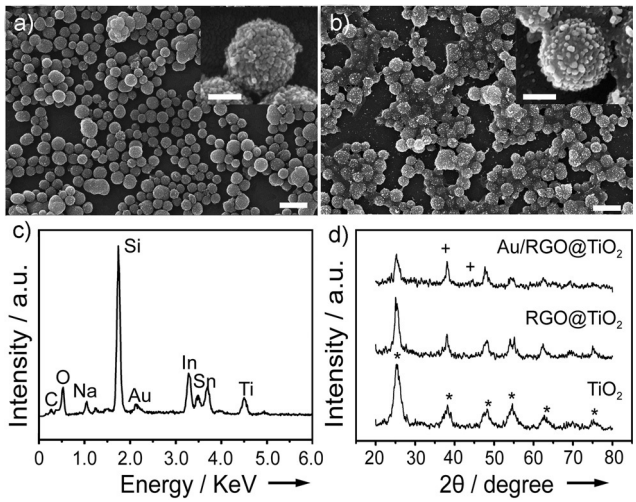

Figure 1. FE-SEM images of a) TiO_2-RGO-ITO and b) Au/RGO@TiO_2-ITO. c) EDX spectrum of Au/RGO@TiO_2-ITO. d) XRD patterns of TiO_2 and its nanocomposites (* represent anatase, + represent Au(111) and Au(200)). Scale bars: 1 μm. Inset scale bars: 200 nm.

according to the previous report,[14] then functionalized with 3-aminopropyltriethoxysilane to render them positively charged (FTIR spectrum shown in Figure S1 in the Supporting Information).[15] The layer-by-layer assembly began with electrochemical deposition of an aqueous GO solution to form a RGO membrane onto the ITO electrode (Scheme 1 a, and SEM image shown in Figure S2 a). Then positively charged TiO_2 NPs (+26 mV) were decorated onto the RGO-ITO by electrophoretic deposition (Scheme 1 b), which was validated by SEM imaging (Figure 1 a) and an EDX spectrum of Ti (Figure S2 b).[16] After that, a RGO@TiO_2 sandwich structure (Scheme 1 c) was formed by electrostatic assembly between positively charged TiO_2 NPs and negatively charged GO, followed by reduction of GO to RGO. The SEM image (Figure S3 a) and the attenuation of the relative Ti intensity in the EDX spectrum (Figure S3 b) both demonstrate that the TiO_2 NPs were successfully wrapped by the RGO membrane. Finally, the Au NPs were deposited onto the RGO@TiO_2 sandwich structure to form Au/RGO@TiO_2-ITO (Scheme 1 d).

The SEM image (Figure 2 b) shows that Au NPs with about 30 nm diameter were deposited on both RGO@TiO_2

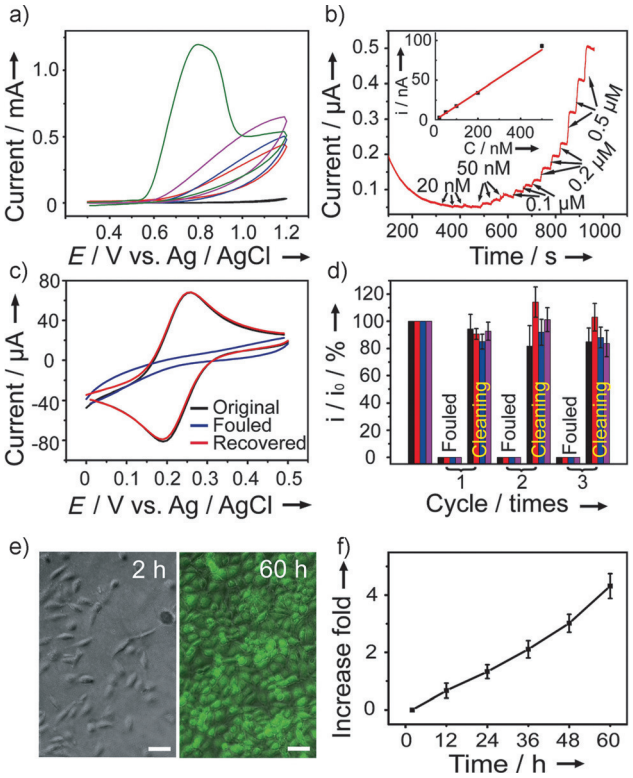

Figure 2. a) Cyclic voltammograms of ITO (black line), RGO-ITO (red line), TiO_2-RGO-ITO (blue line), RGO@TiO_2-ITO (purple line), and Au/RGO@TiO_2-ITO (green line) in the presence of 0.1 mM NO in deaerated PBS solution. b) Amperometric curves of Au/RGO@TiO_2-ITO to a serial of NO concentration in a stirred deaerated PBS solution. A potential of +0.85 V (vs. Ag/AgCl) was applied to the electrode. Inset: Calibration curves of Au/RGO@TiO_2-ITO for increasing the NO concentration. c) Cyclic voltammograms of 1 mM $K_3[Fe(CN)_6]$ in 1 M KCl on the Au/RGO@TiO_2-ITO electrode before fouling (black), after fouling by 5-HT (blue), and after recycling by UV light irradiation. d) Recovery efficiency of Au/RGO@TiO_2-ITO obtained for the $K_3[Fe(CN)_6]$ oxidation current using three cycles. Black line, red line, blue line, and purple line represent 5-HT, PLL, collagen, and CCM. e) Microscopic images of the HUVECs culture on Au/RGO@TiO_2-ITO for different times. Bright field for 2 h and merge of bright field and fluorescence field for 60 h. Scale bar: 50 μm. f) Proliferation curve of HUVECs cultured on Au/RGO@TiO_2-ITO.

and RGO surface. The signal of Au in the EDX spectrum (Figure 1 c) also indicates that the Au NPs were successfully synthesized. The diffraction peaks at 44.38° in the XRD pattern can be indexed to the (200) planes of Au NPs (Figure 2 d). Because of the overlap of 38.28° of Au (111) and 37.8° of TiO_2 (004), Au (111) cannot be distinguished clearly in the XRD pattern (Figure 2 d). However, the intensity ratio between 37.8° and 25.3° increases obviously in Au/RGO@TiO_2 compared to both TiO_2 and RGO@TiO_2, indicating that the peak around 37.8° contains 38.28° of Au (111). The UV/Vis diffuse reflectance spectrum of the TiO_2 nano-

composites is depicted in Figure S3c. As compared to bare TiO_2, the light absorption of RGO@TiO_2 and Au-RGO@TiO_2 increases in the visible light regions which may be attributed to the visible light harvest of RGO and Au NPs.[13b,c] A red-shift absorption edge of RGO@TiO_2 and Au/RGO@TiO_2 was also observed, indicating that band gap of TiO_2 narrowed with the introduction of RGO and Au NPs.[13b,17] Results of photodegradation of Rhodamine 6G (Figure S3d) show that RGO@TiO_2 displayed the best photocatalytic activity, which can be attributed to the separation of photoinduced electrons and holes through the electronic interaction between RGO and TiO_2.[13c,17a] Previous reports showed that the photocatalytic activity of Au-modified TiO_2 was affected by the size and density of Au NPs, and Au NPs smaller than 10 nm with below 2 wt% content were reported to be beneficial for photocatalysis.[13b] In the present work, possibly because of the relatively large size (about 30 nm) and high density of Au NPs, the photocatalytic activity of Au/RGO@TiO_2 decline slightly compared to RGO@TiO_2, but is still obviously higher than that on bare TiO_2. Taking into account of the significantly improved electrochemical activity, Au NPs were essential for the sensor construction in spite of a little photocatalytic activity loss compared to RGO@TiO_2.

To test the electrochemical performance of various electrodes we obtained during the fabrication process, NO was used as a probe because of its vital role in the regulation of physiological and pathological processes.[18] Real-time monitoring of NO with high sensitivity is essential to unravel its various functions.[19] As shown in Figure 2a, Au/RGO@TiO_2-ITO displays the best electrochemical behavior in terms of oxidative potential and amplitude of oxidation current. Without RGO and Au NPs, the TiO_2-ITO electrode displays a poor electrochemical activity (Figure S4), indicating that RGO and Au NPs play important roles in improving the electrochemical performance.[20] Moreover, a synergistic effect was found between RGO and Au NPs, without either RGO or Au NPs, the electrochemical response of RGO@TiO_2-ITO (purple line in Figure 2a) and Au/TiO_2-ITO (blue line in Figure S4b) were both lower than the response of Au/RGO@TiO_2-ITO. This is in agreement with a previous report that synergistic effect occurred between RGO and Au NPs.[21] Amperometric results show that a response of 20 nM NO can be clearly observed on Au/RGO@TiO_2-ITO and the detection limit was calculated to be about 5 nM (signal-to-noise ratio S/N = 3). A linear region from 20 to 500 nM was obtained with a sensitivity of 0.744 $\mu A\,\mu M^{-1}\,cm^{-2}$. Taken together, the electrochemical results demonstrate the high electrochemical performance of Au/RGO@TiO_2-ITO benefiting from the Au NPs–RGO nanocomposite shell.

To assess the recovered performance of the sensor, 5-hydroxytryptamine (5-HT) was used as a model passivation molecule, which can cause a drastic drop in the amperometric or voltammetric signals by accumulation of a non-electrochemically active oxidation product on the electrode surface during electrochemical detection.[12b] Figure 2c (blue line) displays the cyclic voltammogram of $K_3[Fe(CN)_6]$ on fouled Au/RGO@TiO_2-ITO caused by 5-HT oxidation. Compared to the original electrode, the signal on the fouled electrode was sharply attenuated and almost disappeared, but the sensitivity can be recovered efficiently after UV light (12 $mW\,cm^{-2}$) irradiation for 30 minutes. To further investigate the photocatalytic cleaning performance of Au/RGO@TiO_2-ITO towards bio-macromolecules, poly-L-lysine (PLL), collagen, and CCM were used as passivation media, all of which are always involved in cell culture and detection and easy adsorption on electrodes causing passivation. Photocatalytic cleaning results demonstrate that the electrochemical activity can be efficiently recovered (Figure S5) and the recovery percentage was more than 90% (Figure 2d), which can be attributed to the unique structure of the Au/RGO@TiO_2 composite with improves the photocatalytic performance. This indicates that the renewable sensor could potentially be used for recyclable cell culture and detection.

A biocompatible sensing interface is essential for long-term cell culture and detection. Au NPs and graphene were both reported to be biocompatible materials and have been widely applied in bioassays. As shown in Figure 2e and 2f, human umbilical vein endothelical cells (HUVECs) adhere well on the sensor with stretched shape and stably proliferated (Figure S6). Fluorescence staining results display that the cells were almost clearly alive after being cultured for up to 60 h (Figure 2e and Figure S6e), further demonstrating such a sensing interface is biocompatible.

To realize recovered detection of NO released at single-cell level, we fabricated a patterned Au/RGO@TiO_2-ITO micro-electrochemical sensor array (100 μm in diameter) using a photolithographic technique (see the Experiment Section and Figure S7) and layer-by-layer assembly. A fast injection of NO with serial concentrations from a micro-capillary to the sensor was performed to simulate the detection of NO released from cell. The results (Figure 3a and Figure S8) show that the microsensor had excellent responses to NO in both phosphate-buffered saline (PBS) and cell culture medium, and the detection limit was calculated to be about 2 nM in PBS solution and 4 nM in cell culture medium. The sensitivity of the microsensor in the cell culture medium (0.309 $pA\,nM^{-1}$) was about 50% of that in PBS solution (0.667 $pA\,nM^{-1}$), which may be attributed to the partial adsorption of non-electrochemical compounds in the cell culture medium onto the microsensor.

After being seeded on Au/RGO@TiO_2-ITO, HUVECs grew and proliferated well. Fluorescence imaging of HUVECs stained by calcein-AM (green for live cells) and PI (red for dead cells) indicates the excellent viability of the cultured cells (Figure 3b). The release of NO was evoked by stimulating HUVECs with fast injection of L-Arg.[22] An obvious signal (black line in Figure 3c) can be obtained after L-Arg stimulation. To further confirm that the amperometric signal was produced by NO release, a mixture of L-NAME (a specific NOS inhibitor) and L-Arg was used as stimulant and there was no signal produced (red line in Figure 3c). When L-Arg was injected into the sensor without cell, there was also no signal produced (blue line in Figure 3c), excluding the interference of L-Arg.

Because of the adsorption of proteins in culture medium or secretions from cells, the electrode is easy to be passivated. Compared to the original electrode (inset of Figure 3c), the

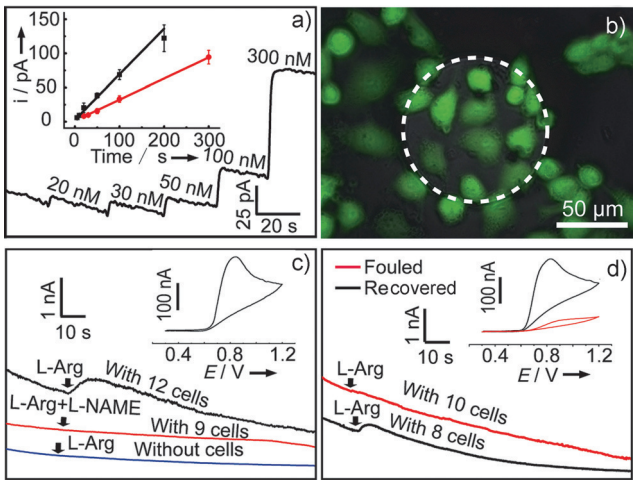

Figure 3. a) The amperometric curve of the Au/RGO@TiO_2-ITO microelectrode for a series of NO concentrations increases at a potential of +0.85 V. Inset: The calibration curve for different concentrations in cell medium (red line) and PBS solution (black line). b) The microscopic image of HUVECs cultured on the Au/RGO@TiO_2-ITO microelectrode stained by calcein-AM (green) and PI (red). The circular area represents the microelectrode with 100 μm diameter. c) Amperometric response of the Au/RGO@TiO_2-ITO microelectrode towards NO released from HUVECs under different conditions. Inset: Cyclic voltammogram of 0.1 mM NO. d) Amperometric response of fouled (red line) and recovered Au/RGO@TiO_2-ITO microelectrodes (black line). Inset: Cyclic voltammograms of 0.1 mM NO on fouled (red line) and recovered sensors (black line).

electrochemical response to NO was drastically attenuated by about 80% (red line of the inset in Figure 3d) after cell culture and detection, which precludes successive and recovered detection (red line in Figure 3d). To regenerate the sensor, photocatalytic cleaning was then carried out with UV irradiation, and results (black line of the inset in Figure 3d) show the electrochemical activity can be recovered by more than 90% of its original response. Then, when we used this recovered electrode to monitor NO release, obvious signals can be obtained again (black line in Figure 3d). Taken together, the results demonstrate that the renewable Au/RGO@TiO_2-ITO micro-electrochemical sensor can efficiently eliminate contaminants after long-term cell culture and detection.

In summary, we developed a highly sensitive and photocatalytic renewable microelectrode array by engineering a Au NPs/RGO@TiO_2 sandwich structure. The Au NPs-RGO composite shell provides a high electrochemical performance, and the encapsulated TiO_2-based composites demonstrate excellent photocatalytic cleaning properties toward absorbed polymers, proteins, and cell culture medium. Recovered monitoring of NO released at single-HUVECs level demonstrates the excellent electrochemical activity and performance of this electrochemical senor, indicating that this kind of renewable electrochemical senor could be successfully applied for recyclable cell culture and detection. Moreover, the strategy presented in this work by combining semiconductor photocatalysts and sensing materials, provides a versatile and efficient way to construct high-performance renewable sensors for biosensing.

Acknowledgements

Supported by the National Natural Science Foundation of China (grant numbers 21375099, 91017013), doctoral funds of Ministry of Education of China (grant number 20120141110031), and the Fundamental Research Funds for the Central Universities (grant number 2042014kf0192),

Keywords: electrochemistry · nitric oxide · recyclable detection · photocatalytic cleaning · renewable electrochemical sensors

How to cite: *Angew. Chem. Int. Ed.* **2015**, *54*, 14402–14406
Angew. Chem. **2015**, *127*, 14610–14614

[1] a) R. M. Wightman, *Science* **2006**, *311*, 1570–1574; b) A. Schulte, W. Schuhmann, *Angew. Chem. Int. Ed.* **2007**, *46*, 8760–8777; *Angew. Chem.* **2007**, *119*, 8914–8933; c) C. Amatore, S. Arbault, M. Guille, F. Lemaitre, *Chem. Rev.* **2008**, *108*, 2585–2621; d) Y. Huang, D. Cai, P. Chen, *Anal. Chem.* **2011**, *83*, 4393–4406; e) X. T. Zheng, C. M. Li, *Chem. Soc. Rev.* **2012**, *41*, 2061–2071; f) M. Zhang, P. Yu, L. Mao, *Acc. Chem. Res.* **2012**, *45*, 533–543; g) J.-T. Liu, L.-S. Hu, Y.-L. Liu, R.-S. Chen, Z. Cheng, S.-J. Chen, C. Amatore, W.-H. Huang, K.-F. Huo, *Angew. Chem. Int. Ed.* **2014**, *53*, 2643–2647; *Angew. Chem.* **2014**, *126*, 2681–2685; h) Y.-T. Li, S.-H. Zhang, L. Wang, R.-R. Xiao, W. Liu, X.-W. Zhang, Z. Zhou, C. Amatore, W.-H. Huang, *Angew. Chem. Int. Ed.* **2014**, *53*, 12456–12460; *Angew. Chem.* **2014**, *126*, 12664–12668; i) W.-W. Zhao, J.-J. Xu, H.-Y. Chen, *Chem. Soc. Rev.* **2015**, *44*, 729–741.

[2] a) M. Hawley, S. Tatawawadi, S. Piekarski, R. Adams, *J. Am. Chem. Soc.* **1967**, *89*, 447–450; b) M. Z. Wrona, G. Dryhurst, *Bioorg. Chem.* **1990**, *18*, 291–317; c) X. Yang, J. Kirsch, J. Fergus, A. Simonian, *Electrochim. Acta* **2013**, *94*, 259–268.

[3] a) I. Hafez, K. Kisler, K. Berberian, G. Dernick, V. Valero, M. G. Yong, H. G. Craighead, M. Lindau, *Proc. Natl. Acad. Sci. USA* **2005**, *102*, 13879–13884; b) A. Hai, J. Shappir, M. E. Spira, *Nat. Methods* **2010**, *7*, 200–202; c) A. Meunier, O. Jouannot, R. Fulcrand, I. Fanget, M. Bretou, E. Karatekin, S. Arbault, M. Guille, F. Darchen, F. Lemaître, C. Amatore, *Angew. Chem. Int. Ed.* **2011**, *50*, 5081–5084; *Angew. Chem.* **2011**, *123*, 5187–5190; d) J. Wang, R. L. Trouillon, Y. Lin, M. I. Svensson, A. G. Ewing, *Anal. Chem.* **2013**, *85*, 5600–5608; e) Y.-L. Liu, X.-Y. Wang, J.-Q. Xu, C. Xiao, Y.-H. Liu, X.-W. Zhang, J.-T. Liu, W.-H. Huang, *Chem. Sci.* **2015**, *6*, 1853–1858.

[4] a) L.-M. Li, W. Wang, S.-H. Zhang, S.-J. Chen, S.-S. Guo, O. Français, J.-K. Cheng, W.-H. Huang, *Anal. Chem.* **2011**, *83*, 9524–9530; b) W. Harreither, R. Trouillon, P. Poulin, W. Neri, A. G. Ewing, G. Safina, *Anal. Chem.* **2013**, *85*, 7447–7453; c) J. Patel, L. Radhakrishnan, B. Zhao, B. Uppalapati, R. C. Daniels, K. R. Ward, M. M. Collinson, *Anal. Chem.* **2013**, *85*, 11610–11618.

[5] a) C. Spégel, A. Heiskanen, J. Acklid, A. Wolff, R. Taboryski, J. Emnéus, T. Ruzgas, *Electroanalysis* **2007**, *19*, 263–271; b) C. Hu, C. Yang, S. Hu, *Electrochem. Commun.* **2007**, *9*, 128–134; c) P. Hashemi, E. C. Dankoski, J. Petrovic, R. B. Keithley, R. M. Wightman, *Anal. Chem.* **2009**, *81*, 9462–9471; d) Y. S. Singh, L. E. Sawarynski, P. D. Dabiri, W. R. Choi, A. M. Andrews, *Anal. Chem.* **2011**, *83*, 6658–6666.

[6] a) X. Yang, J. Kirsch, E. V. Olsen, J. W. Fergus, A. L. Simonian, *Sens. Actuators B* **2013**, *177*, 659–667; b) C. Pirvu, C. C. Manole, *Electrochim. Acta* **2013**, *89*, 63–71.

[7] a) J. Xu, Q. Chen, G. M. Swain, *Anal. Chem.* **1998**, *70*, 3146–3154; b) J. H. Luong, K. B. Male, J. D. Glennon, *Analyst* **2009**, *134*, 1965–1979.

[8] A. G. Zestos, C. B. Jacobs, E. Trikantzopoulos, A. E. Ross, B. J. Venton, *Anal. Chem.* **2014**, *86*, 8568–8575.

[9] a) L. M. Fischer, M. Tenje, A. R. Heiskanen, N. Masuda, J. Castillo, A. Bentien, J. Émneus, M. H. Jakobsen, A. Boisen, *Microelectron. Eng.* **2009**, *86*, 1282 – 1285; b) V. Bhalla, S. Carrara, C. Stagni, B. Samorì, *Thin Solid Films* **2010**, *518*, 3360 – 3366.

[10] a) P. Takmakov, M. K. Zachek, R. B. Keithley, P. L. Walsh, C. Donley, G. S. McCarty, R. M. Wightman, *Anal. Chem.* **2010**, *82*, 2020 – 2028; b) R. Kiran, E. Scorsone, P. Mailley, P. Bergonzo, *Anal. Chem.* **2012**, *84*, 10207 – 10213.

[11] a) S. Liu, J. Yu, M. Jaroniec, *Chem. Mater.* **2011**, *23*, 4085 – 4093; b) H. Tong, S. Ouyang, Y. Bi, N. Umezawa, M. Oshikiri, J. Ye, *Adv. Mater.* **2012**, *24*, 229 – 251; c) H. Kisch, *Angew. Chem. Int. Ed.* **2013**, *52*, 812 – 847; *Angew. Chem.* **2013**, *125*, 842 – 879; d) H. Wang, L. Zhang, Z. Chen, J. Hu, S. Li, Z. Wang, J. Liu, X. Wang, *Chem. Soc. Rev.* **2014**, *43*, 5234 – 5244; e) T. Hisatomi, J. Kubota, K. Domen, *Chem. Soc. Rev.* **2014**, *43*, 7520 – 7535.

[12] a) X. Li, G. Chen, L. Yang, Z. Jin, J. Liu, *Adv. Funct. Mater.* **2010**, *20*, 2815 – 2824; b) L. Hu, K. Huo, R. Chen, B. Gao, J. Fu, P. K. Chu, *Anal. Chem.* **2011**, *83*, 8138 – 8144; c) X. Li, H. Hu, D. Li, Z. Shen, Q. Xiong, S. Li, H. J. Fan, *ACS Appl. Mater. Interfaces* **2012**, *4*, 2180 – 2185; d) C. Wen, F. Liao, S. Liu, Y. Zhao, Z. Kang, X. Zhang, M. Shao, *Chem. Commun.* **2013**, *49*, 3049 – 3051.

[13] a) J. Yu, G. Dai, Q. Xiang, M. Jaroniec, *J. Mater. Chem.* **2011**, *21*, 1049 – 1057; b) A. Primo, A. Corma, H. Garcia, *Phys. Chem. Chem. Phys.* **2011**, *13*, 886 – 910; c) Q. Xiang, J. Yu, M. Jaroniec, *Chem. Soc. Rev.* **2012**, *41*, 782; d) D. Chen, H. Feng, J. Li, *Chem. Rev.* **2012**, *112*, 6027; e) M.-Q. Yang, N. Zhang, M. Pagliaro, Y.-J. Xu, *Chem. Soc. Rev.* **2014**, *43*, 8240 – 8254; f) W.-W. Zhao, J.-J. Xu, H.-Y. Chen, *Chem. Rev.* **2014**, *114*, 7421 – 7441; g) Z. Sun, X. Huang, M. Muhler, W. Schuhmann, E. Ventosa, *Chem. Commun.* **2014**, *50*, 5506 – 5509; h) Q. Xiang, B. Cheng, J. Yu, *Angew. Chem. In. Ed.* **2015**, *54*, 11350 – 11366; *Angew. Chem.* **2015**, *127*, 11508 – 11524.

[14] J. S. Lee, K. H. You, C. B. Park, *Adv. Mater.* **2012**, *24*, 1084 – 1088.

[15] L. Valentini, M. Cardinali, J. Kenny, *Carbon* **2010**, *48*, 861 – 867.

[16] R. Morand, C. Lopez, M. Koudelka-Hep, P. Kedzierzawski, J. Augustynski, *J. Phys. Chem. B* **2002**, *106*, 7218 – 7224.

[17] a) H. Zhang, X. Lv, Y. Li, Y. Wang, J. Li, *ACS Nano* **2010**, *4*, 380 – 386; b) Y. Zhang, Z.-R. Tang, X. Fu, Y.-J. Xu, *ACS Nano* **2011**, *5*, 7426 – 7435.

[18] a) F. Murad, *Angew. Chem. Int. Ed.* **1999**, *38*, 1856 – 1868; *Angew. Chem.* **1999**, *111*, 1976 – 1989; b) D. A. Riccio, M. H. Schoenfisch, *Chem. Soc. Rev.* **2012**, *41*, 3731 – 3741; c) A. W. Carpenter, M. H. Schoenfisch, *Chem. Soc. Rev.* **2012**, *41*, 3742 – 3752.

[19] a) S. Isik, W. Schuhmann, *Angew. Chem. Int. Ed.* **2006**, *45*, 7451 – 7454; *Angew. Chem.* **2006**, *118*, 7611 – 7614; b) J. H. Shin, B. J. Privett, J. M. Kita, R. M. Wightman, M. H. Schoenfisch, *Anal. Chem.* **2008**, *80*, 6850 – 6859; c) P. N. Coneski, M. H. Schoenfisch, *Chem. Soc. Rev.* **2012**, *41*, 3753 – 3758; d) P. Rivera Gil, C. Vazquez-Vazquez, V. Giannini, M. P. Callao, W. J. Parak, M. A. Correa-Duarte, R. A. Alvarez-Puebla, *Angew. Chem. Int. Ed.* **2013**, *52*, 13694 – 13698; *Angew. Chem.* **2013**, *125*, 13939 – 13943.

[20] a) Y. Liu, X. Dong, P. Chen, *Chem. Soc. Rev.* **2012**, *41*, 2283 – 2307; b) C. X. Guo, S. R. Ng, S. Y. Khoo, X. Zheng, P. Chen, C. M. Li, *ACS Nano* **2012**, *6*, 6944 – 6951; c) S. L. Ting, C. X. Guo, K. C. Leong, D.-H. Kim, C. M. Li, P. Chen, *Electrochim. Acta* **2013**, *111*, 441 – 446.

[21] J. Li, J. Xie, L. Gao, C. M. Li, *ACS Appl. Mater. Interfaces* **2015**, *7*, 2726 – 2734.

[22] R. M. J. Palmer, D. S. Ashton, S. Moncada, *Nature* **1988**, *333*, 664 – 666.

Received: August 7, 2015
Revised: September 9, 2015
Published online: October 2, 2015

